Supporting Information for

Freezing of Gelled Suspensions: a Facile Route Towards Mesoporous TiO_2 Particles for High-Capacity Li-Ion Electrodes

Clara Minas[a], Felix Rechberger[b], Elena Tervoort[a, b], Fabio L. Bargardi[a], Juliette Billaud[c], Markus Niederberger[b§], Florian Bouville[a, d]*, André R. Studart[a+]

[a] Complex Materials, Department of Materials, ETH Zürich, 8093 Zürich, Switzerland
* E-mail: f.bouville@imperial.ac.uk
+ E-mail: andre.studart@mat.ethz.ch
[b] Laboratory for Multifunctional Materials, Department of Materials, ETH Zürich, 8093 Zürich, Switzerland.
§ E-mail: markus.niederberger@mat.ethz.ch
[c] Electrochemical Laboratory, Paul Scherrer Institut, CH-5232 Villigen PSI, Switzerland
[d] Now at: Center for Advanced Structural Ceramics, Department of Materials, Imperial College London, Royal School of Mines, SW7 2AZ London, United Kingdom

S1. Packing fraction of the lamellae in cryogel and pre-gelled cryogel samples

The packing fraction in the lamellae of unidirectionally frozen samples is determined by the packing fraction at which the ice starts growing into the regions of the particle network. This *breakthrough* point has been modelled as the point at which the osmotic force of the suspension exceeds the capillary drag force, which pushes the particles in front of the solidification front.[1,2] As such, the packing fraction at breakthrough is defined as

$$\Phi_B = \Phi_m - (\frac{k_b T}{4\pi R^2 \gamma})^{1/3} = \Phi_m - W, \quad \text{(S1)}$$

where Φ_m represents the maximum packing fraction, k_b the Boltzmann constant, R the particles radius, T the temperature, and γ the surface tension of the liquid-solid interface. W represents the deviation from the maximum packing fraction.

$$W = (\frac{k_b T}{4\pi R^2 \gamma})^{1/3} \quad \text{(S2)}$$

For 273 K, a surface tension 0.07 J/m^2 (water) and a particle diameter of 5 nm, equation (S2) results in the theoretically expected deviation from maximum packing, W_{th} = 0.056.

The experimentally observed packing fraction can be calculated using

$$\Phi = 1 - P, \quad \text{(S3)}$$

where the porosity (P) is experimentally derived using BET measurements.
Ambient drying of the pre-gelled wet samples can be assumed to result in the maximum packing fraction. Thus, the experimentally derived value for the packing fraction of the xerogel is equal to Φ_m.
The values of Φ, as calculated using equation (S3), and the deviation from the maximum packing fraction (W_{BET}), as calculated using equation (S1), for the cryogel and the pre-gelled cryogel are listed in Table S1.

Table S1: Packing fraction (Φ) and the theoretical expected (W_{th}) and experimentally observed (W_{BET}) deviation from the maximum packing fraction of the xerogel, cryogel and non-gelled cryogel as obtained in this work.

	xerogel	cryogel	pre-gelled cryogel
Φ	0.6883	0.6454	0.5069
W_{th}		0.0560	0.0560
W_{BET}		0.0429	0.1814

W_{BET} for the cryogel is in good agreement to the expected deviation from the maximum packing (W_{th}) fraction as calculated using equation (S2). By contrast, W_{BET} for the pre-gelled cryogel is

more than three times larger than W_{th} indicating that the balance of osmotic and capillary pressure does not sufficiently describe the breakthrough phenomena for the gelled system.

S2. HRTEM and STEM analysis

TEM was performed on a XFEG FEI-Talos. The samples for TEM characterisation were dispersed in chloroform and a drop of the suspension was placed onto a carbon coated copper grid lying on a filter paper, followed by drying in air at room temperature.

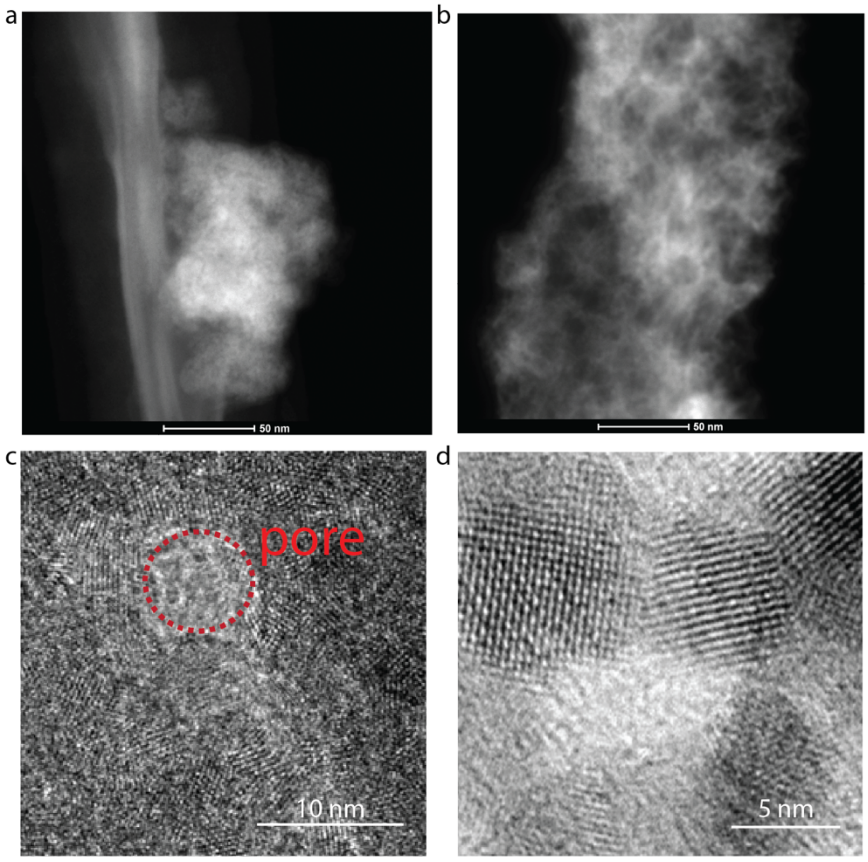

Figure S1. STEM and HRTEM of the aerogel and pre-gelled cryogel. a. STEM of the pre-gelled cryogel and b. of the aerogel. c. HRTEM of the pre-gelled cryogel d. close-up view showing particle crystallinity.

S3. N_2-Adsorption isotherms

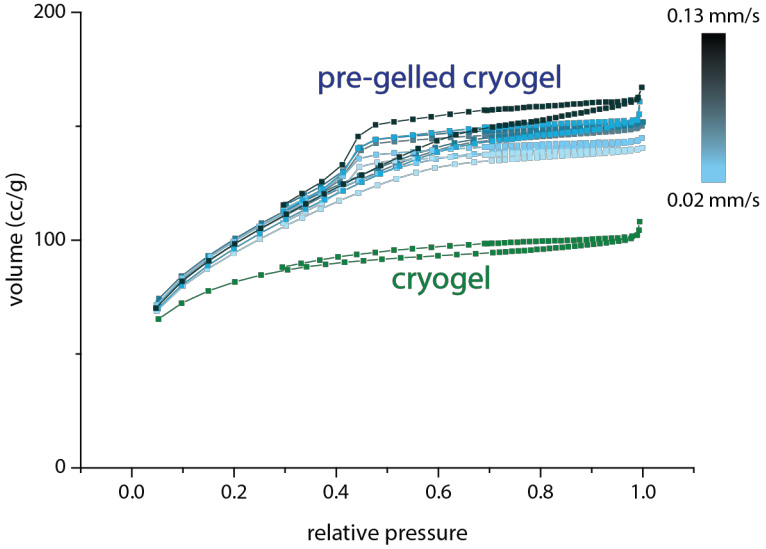

Figure S2. The N_2 adsorption-desorption isotherms for pre-gelled cryogels frozen at speed varying from 0.02 mm/s to 0.13 mm/s compared to cryogel.

S4. Powder analysis

X-ray diffraction was carried out on the different powders used for the fabrication of hierarchical porous anodes for Li-ion batteries presented in this work (Figure 4). The diffractograms in Figure S1 show no differences in crystallinity or crystal size between the differently processed TiO_2 powders.

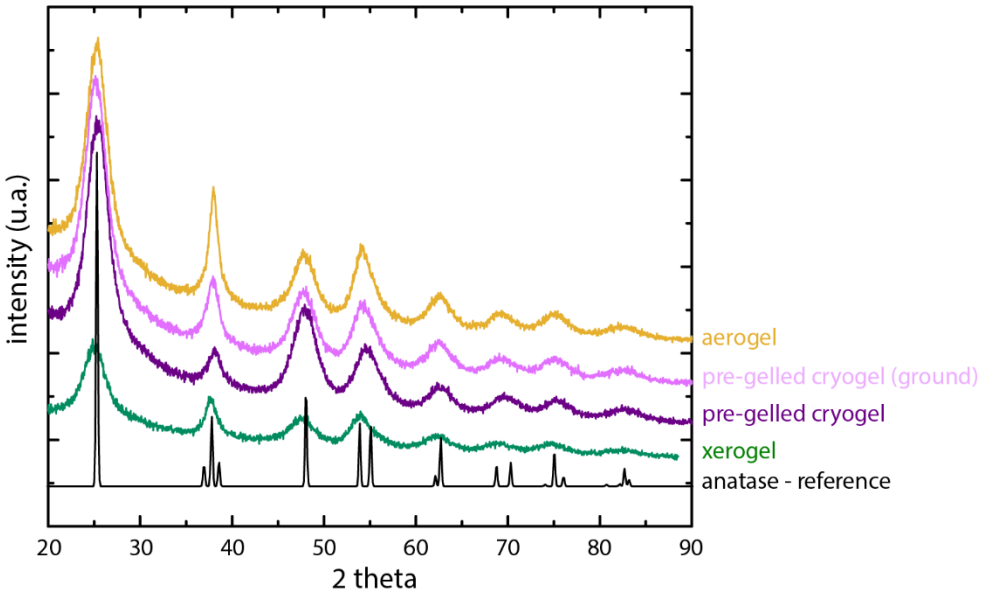

Figure S3. X-ray diffractograms of powders used for electrode fabrication in this work as well as an anatase reference (JCPDS Card 21-1272).

S5 Charge-discharge curves of half-cell

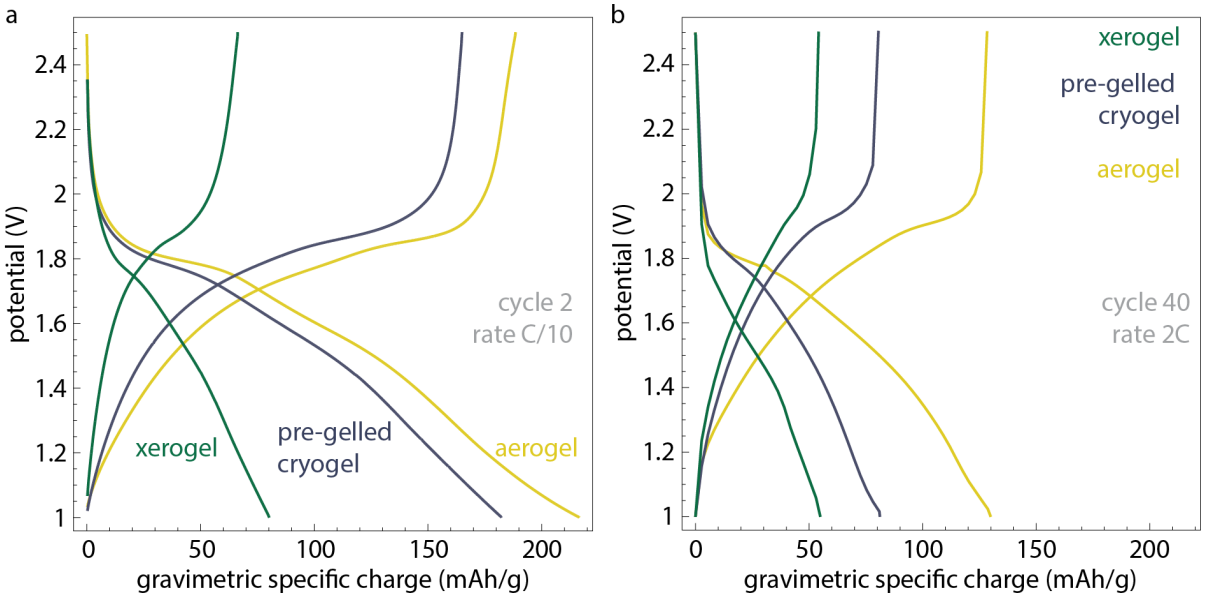

Figure S4. Charge-discharge curves for the three architectures at two cycling rate: (a) C/10 and (b) 2C.

S6. Performance comparison with literature values

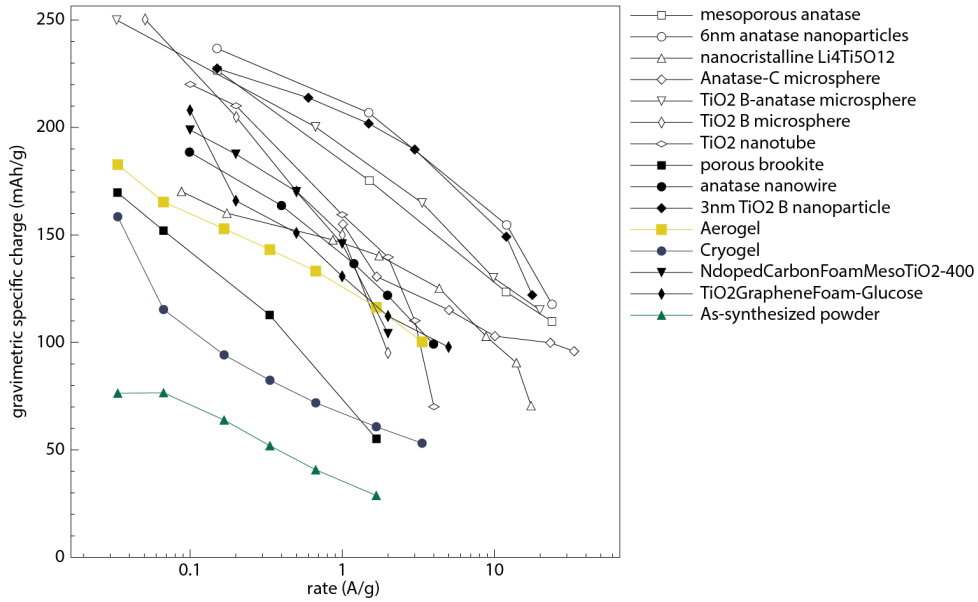

Figure S5. Comparison of the specific electrochemical performances of the aerogel, pre-gelled cryogel, and nanopowder with literature values for TiO_2 structured and related compounds. Adapted from references[3–6].

S7. Long term stability

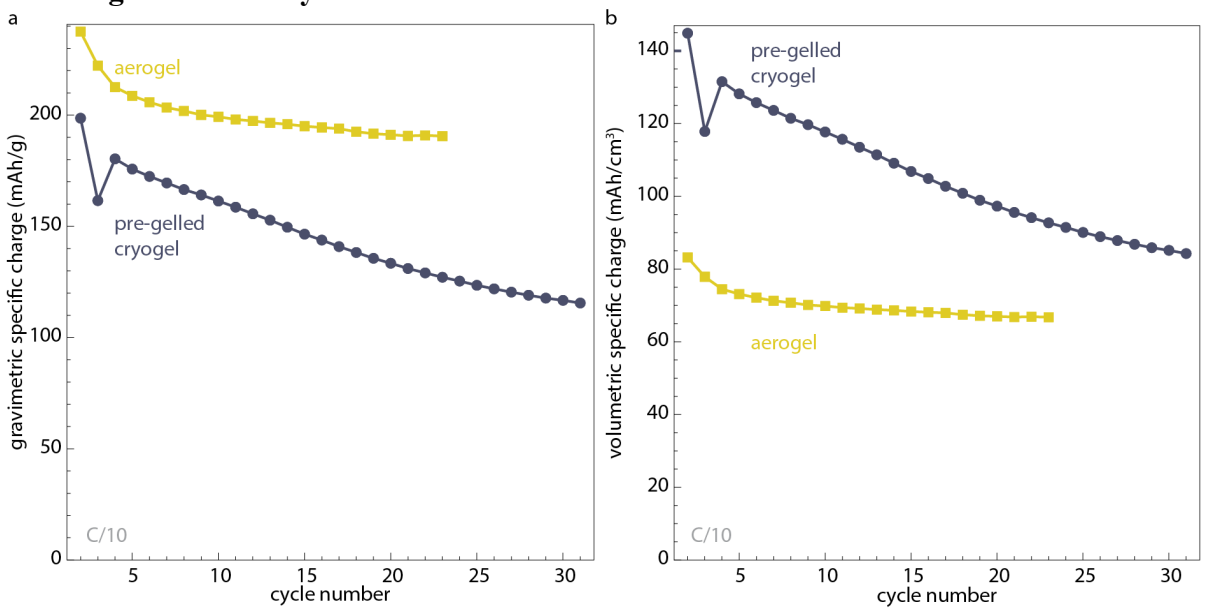

Figure S6. Cycling stability at C/10 for the aerogel and pre-gelled cryogel powders. a. Gravimetric specific charge and b. volumetric specific charge as a function of the number of cycles.

References

(1) Shanti, N. O.; Araki, K.; Halloran, J. W. Particle Redistribution During Dendritic Solidification of Particle Suspensions. *J. Am. Ceram. Soc.* **2006**, *89*, 2444–2447.

(2) Deville, S.; Bernard-Granger, G. Influence of Surface Tension, Osmotic Pressure and Pores Morphology on the Densification of Ice-Templated Ceramics. *J. Eur. Ceram. Soc.* **2011**, *31*, 983–987.

(3) Ren, Y.; Hardwick, L. J.; Bruce, P. G. Lithium Intercalation into Mesoporous Anatase with an Ordered 3D Pore Structure. *Angew. Chemie* **2010**, *49*, 2570–2574.

(4) Ren, Y.; Liu, Z.; Pourpoint, F.; Armstrong, a. R.; Grey, C. P.; Bruce, P. G. Nanoparticulate TiO_2(B): An Anode for Lithium-Ion Batteries. *Angew. Chemie* **2012**, *124*, 2206–2209.

(5) Chu, S.; Zhong, Y.; Cai, R.; Zhang, Z.; Wei, S.; Shao, Z. Mesoporous and Nanostructured TiO_2 Layer with Ultra-High Loading on Nitrogen-Doped Carbon Foams as Flexible and Free-Standing Electrodes for Lithium-Ion Batteries. *Small* **2016**, No. 48, 6724–6734.

(6) Qiu, B.; Xing, M.; Zhang, J. Mesoporous TiO_2 Nanocrystals Grown in Situ on Graphene Aerogels for High Photocatalysis and Lithium-Ion Batteries. *J. Am. Chem. Soc.* **2014**, *136*, 5852–5855.